Energy 166 (2019) 1106–1119

Contents lists available at ScienceDirect

Energy

journal homepage: www.elsevier.com/locate/energy

Numerical analysis of gas production from layered methane hydrate reservoirs by depressurization

Yongchang Feng [a, *], Lin Chen [b], Anna Suzuki [a], Takuma Kogawa [c], Junnosuke Okajima [a], Atsuki Komiya [a], Shigenao Maruyama [a]

[a] Institute of Fluid Science, Tohoku University, Sendai, Miyagi, 980-8577, Japan
[b] Institute of Engineering Thermophysics, Chinese Academy of Sciences, Beijing, 100190, China
[c] National Institute of Technology, Hachinohe College, Tamonoki, Hachinohe, 039-1192, Japan

ARTICLE INFO

Article history:
Received 2 September 2018
Received in revised form
26 October 2018
Accepted 28 October 2018
Available online 29 October 2018

Keywords:
Methane hydrate
Layered structure
Depressurization
Gas production

ABSTRACT

Many natural methane hydrate (MH) reservoirs are heterogeneous and are characterized by a layered structure. In this study, we numerically investigate gas production from a multi-layered hydrate reservoir by depressurization through a single vertical and a single horizontal well. This layered MH reservoir is constructed based on field test data at the AT1 site of the Eastern Nankai Trough in Japan, and involves three hydrate-bearing layers (HBLs): Upper HBL-1, middle HBL-2, and lower HBL-3. The simulation results indicate that the horizontal well shows a better gas production performance in comparison to the vertical well. Over a production duration of two years, the average gas production rate by using the horizontal well reached 7.3×10^4 ST m^3/d, which is 5.7 times higher than that by using the vertical well. However, the gas-to-water ratio for both the vertical and horizontal well cases is low in absolute terms. Sensitivity analysis of gas production by the horizontal well indicates that both the very higher and lower levels of permeability in HBL-2 and hydrate saturation in HBL-3 are unfavorable for long-term gas production. In addition, decrease of vertical permeability in HBL-1 and HBL-3 can lead to lower gas production efficiency.

1. Introduction

Methane hydrate (MH) is crystalline solid composed of water and methane gas. Naturally occurring MH has been found to exist widely in oceanic sediments and permafrost regions where both the temperature and pressure conditions are suitable for its formation and stability [1]. It is considered one of the most promising alternative energy resources because of its high-energy density, abundance in nature and cleanness [2–4]. Over the last few decades, much attention has been focused on the problems of extracting gas from methane hydrate reservoirs due to the increased environment pollution and the expansion of the energy consumption pressure in the world. Other than these, many systems for comprehensive methane hydrate utilization process have been proposed, such as the low CO_2 emission power generation system by Maruyama et al. [5]. It is greatly expected that MH could be efficiently explored and economically exploited in the near future.

Gas production from methane hydrate is a complex process involving heat transfer, multi-phase fluids (gas, liquid, ice and hydrate) flow, and endothermic reaction. According to the phase-equilibrium curve of methane hydrate, there are three basic techniques for gas production from hydrate reservoirs [3,4]: Depressurization, thermal stimulation and inhibitor injection. Among these production methods, depressurization is accepted as the most promising production strategy for the hydrate reservoirs with high permeability in the hydrate-bearing layer (HBL) due to its simplicity and its technical and economic effectiveness [6–9]. This method is conducted by decreasing the pressure in the production well to a level below the equilibrium condition and making the methane hydrate unstable. In recent years, a number of numerical and experimental studies [10–16] on depressurization-induced gas production from methane hydrate has been carried out at different scales (core-scale, pilot-scale and reservoir-scale), and suggest that the initial permeability and temperature are the two key factors controlling MH dissociation during depressurization.

* Corresponding author.
E-mail addresses: feng.yongchang.d4@tohoku.ac.jp, feng.y.c@stu.xjtu.edu.cn (Y. Feng).

https://doi.org/10.1016/j.energy.2018.10.184
0360-5442/

With the rapid development of computer technology and the further understanding of the mechanism of hydrate dissociation in complex geological media, numerical simulation became a better way to evaluate the gas production potential from MH reservoirs and find the production strategies. However due to the absence of substantial well data, most of the simulation models [17–19] assume reservoirs to be homogeneous. In fact, natural MH reservoirs are heterogeneous due to several factors, such as irregular-shaped particles, stress-induced effects and aligned cracks [20–24], and many of them are characterized by a layered structure. This may be caused by the depositional layering at different geological time scales [22]. Examples are the methane hydrate reservoirs in Shenhu Area of South China Sea [25] and in the Eastern Nankai Trough, Japan [7,26]. This layered structure can lead to the anisotropy of reservoir permeability that may ultimately affect the heat and mass transfer during gas production from MH reservoirs. Thus, the consideration of layered structure effect is critical to conduct exact numerical simulation in the analysis of reservoir-scale hydrate dissociation. On the other hand, most field test data [7,27] and simulations [9,26,28,29] indicate that the gas production rate from actual hydrate reservoirs is too low to meet the requirement of commercial production when using vertical well, and the horizontal well can be more favorable for gas production.

In this study, gas production from layered MH reservoir was investigated. First, we constructed a multi-layered MH reservoir model based on the logging and pressure core data at the AT1 site of the Eastern Nankai Trough, Japan. Based on the numerical simulation matched with the recorded field test data in short-term production, we further investigated long-term gas production behavior by depressurization through a single vertical well and a single horizontal well, respectively. In addition, the sensitivity of gas production using horizontal well to the main system parameters was also analysed. It is hoped that the research of this paper could help to obtain a clearer understanding of gas production from natural hydrate reservoirs.

2. Multi-layered hydrate reservoir in the Eastern Nankai Trough

2.1. General reservoir information

Since 1996, the Eastern Nankai Trough (as shown in Fig. 1 (a)), one of the most potential resource-rich areas of methane hydrate in Japan, has been chosen for MH surveys by the Japanese Ministry of Economy, Trade and Industry (METI). After years of exploration surveys and studies, more than ten prospective MH-concentrated zones (MHCZs) have been identified in this areas [30]. The total amount of methane hydrate in these MHCZs is estimated at an average value of 5.7×10^{11} m^3, which accounts for around half of the methane hydrate within the survey areas. Studies of MH-bearing core samples from this area show that the purity of produced methane gas can reach above 99%, and most of the methane gas is biogenic methane [31,32].

The β - MHCZ, as shown in Fig. 1 (b), is one of the MHCZs in the Eastern Nankai Trough, and was discovered in the northwestern slope of Daini Atsumi Knoll in 2004. This MHCZ has an area of approximately 12 km^2 with the water depth ranging from 857 to 1405 m. Geophysical logging and coring analyses indicated that the MHCZ has a thickness of several tens of meters [33]. In 2012, a test site in the β - MHCZ, referred to as AT1, was selected for the offshore production test by the Research Consortium for Methane Hydrate Resources in Japan (MH 21) based on analysis of the geographical structure and the hydrate-bearing system characteristics, such as water depth, the pressure-temperature condition of hydrate formation, and the existence of sealing layers. Methane hydrate was confirmed in sandy turbidite sediment within 300 m below the seafloor at a water depth of approximately 1000 m. The hydrate-containing sediment is about 60 m thick. Then, a continuous 6-day gas production was conducted at AT1 by depressurization method in 2013, which was the world's first offshore production test.

2.2. Multi-layered hydrate reservoir

According to the analyses of well logging and pressure core data obtained from the AT1 site, the detected MH reservoir shows good lateral continuity of lithofacies. The lithology mainly includes sand, silt, and clay, of which methane hydrate is found to mainly exist in the sandy layer, as shown in Fig. 2. This MH reservoir is composed of an approximately 60m-thick MHCZ, a 20m-thick muddy zone above the MHCZ, and a water-bearing zone below the MHCZ. Based on the lithofacies, the MHCZ can be further divided into three thick zones: Upper MHCZ, middle muddy zone, and lower MHCZ. The upper MHCZ is composed of thin alternations of sand and silt

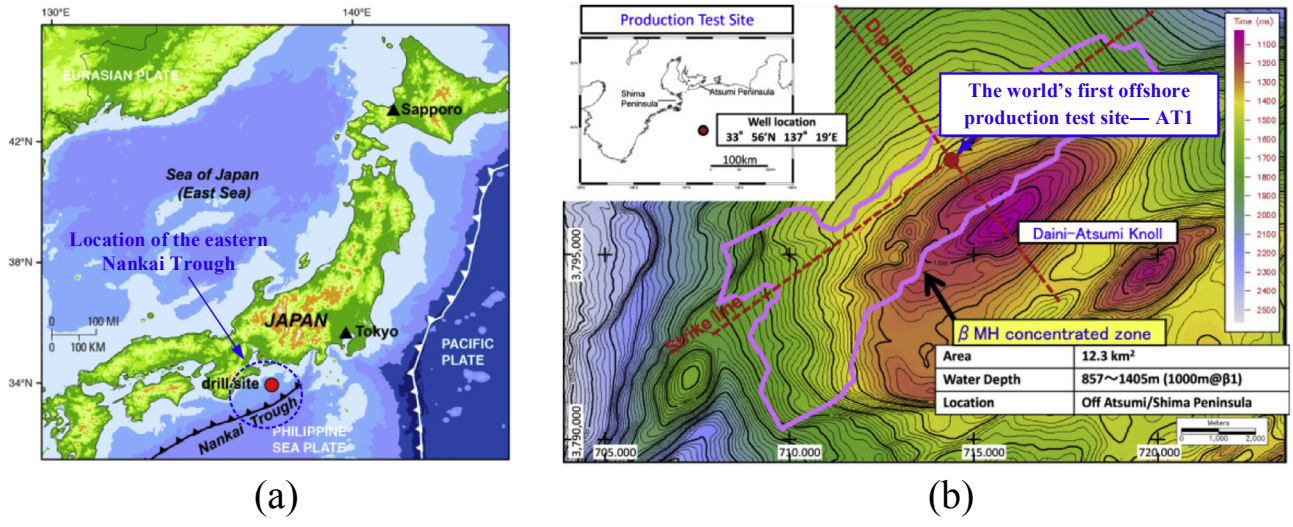

Fig. 1. Sketch maps of (a) the Eastern Nankai Trough (modified from USGS photo [34]) and (b) the β - MHCZ (modified from Fujii et al. [21]).

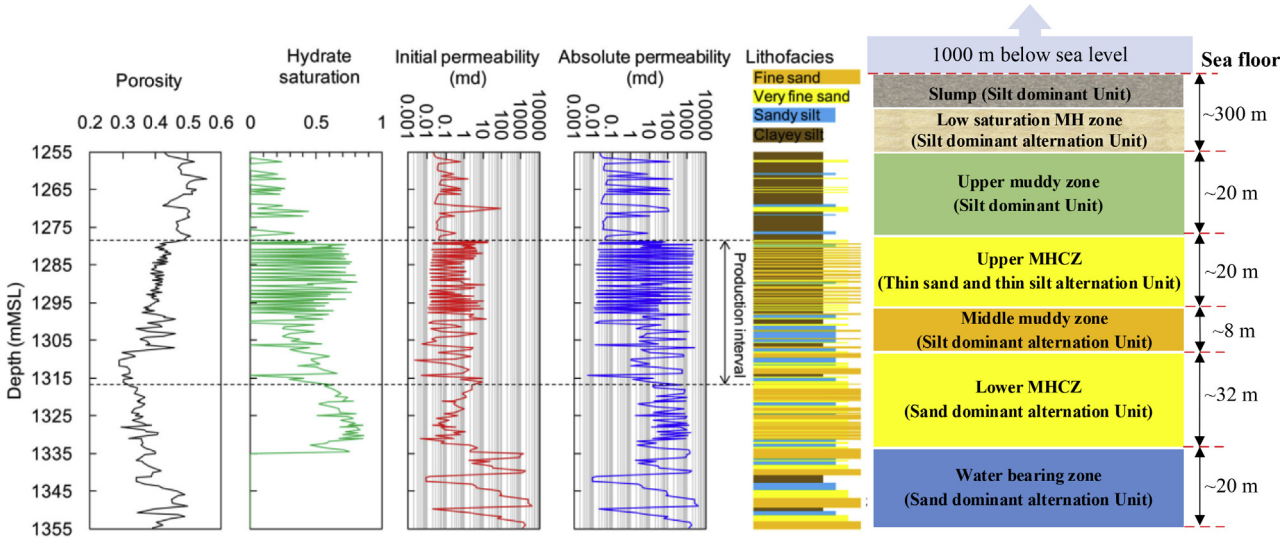

Fig. 2. Depth profiles of effective porosity, hydrate saturation, and initial effective and absolute permeability with lithofacies (modified from Konno et al. [7]).

layers. The middle muddy zone is the same as the upper MHCZ, but has a higher ratio of silt-to-sand layers. The lower MHCZ is composed of relatively thick sand-dominant sequences. As opposed to the typical Class 3 reservoirs, this MH reservoir is characterized by the absence of sealing layers (impermeable layers) below the MHCZ, which is connected to a water-bearing zone in the lower part. This can make depressurization and water management challenging during gas production. Therefore in the field production test in 2013, the production well was drilled at about 40 m from the top of the upper MHCZ to the upper part of the lower MHCZ, which was about 20 m above the water-bearing layer. In addition, as shown in Fig. 2 (referred from Konnol et al. [7], the reservoir is divided into 202 layers based on the lithofacies), the MH reservoir has different porosity, hydrate saturation, initial permeability, and absolute permeability in each layer. Therefore, the development of suitable geological model and key petrophysical parameters is critical for the numerical simulation of gas production from this multi-layered hydrate reservoir. A more detailed description and geological analysis of the MH reservoir can be found in Fujii et al. [21] and Konno et al. [7]. The present study focused on the simulation of gas production from layered MH reservoir at the AT1 site.

3. Numerical model and simulation approach

3.1. Model construction and well design

In this study, we first constructed a multi-layered MH reservoir model based on the real geological survey data [7,21] and our previous studies [26] related to the MH sediment at the AT1 site of the Eastern Nankai Trough. This is a complex hydrate reservoir, in which a 60 m-thick hydrate-bearing layer (HBL) is confined by an impermeable overburden (OB) and a permeable underburden (UB) with the same thickness of 20 m. The HBL contains three sub-HBLs: HBL-1(20 m thick), HBL-2(8 m thick), and HBL-3(32 m thick), which correspond to the upper MHCZ, middle muddy zone, and lower MHCZ in Fig. 2.

Two computational domains are considered in this numerical study, namely, a cylindrical reservoir model for vertical well system (as shown in Fig. 3(a)) and a rectangular reservoir model for horizontal well system (as shown in Fig. 3(b)). The hydrate deposit volume, initial conditions, and production pressure are the same in each simulation configuration. The cylindrical geometry is applied to validate the numerical code and model employed in this study and estimate the long-term gas production performance by vertical well, and the second one is taken into account to investigate the gas production performance by horizontal well and determine the important factors affecting production.

In this numerical study, the radius and height of the cylindrical model are set to be $r_{max} = 200$ m and $L_z = 100$ m, respectively, and a single vertical well with radius $r_w = 0.1$ is located in the centre of the model. The production interval is 38 m and is completed from the top of HBL-1 to the upper part of HBL-3, which is consistent with the field test in the Eastern Nankai Trough in 2013. Because of the symmetry of cylindrical model, only a 2D cylindrical section is simulated in this work, as shown in Fig. 3(a). The rectangular model with the same MH volume has a cubic footprint with $L_x = L_y = L_z = 354$ m. A single horizontal well with radius $r_w = 0.1$ m is arranged along the *Y* direction ($L_w = 354$ m) and placed at the top of the HBL ($L_d = 0.1$ m), considering the gas buoyancy and accumulation at this location and minimizing effectively water production. Assuming uniformity of reservoir properties along the length of horizontal well (*Y* direction), only a 2D section of unite thickness on the *X-Z* plane is considered in this study. In addition, the *X-Z* plane is symmetrical along the vertical direction. Therefore, we only model half of the section ($0\,m < x < 177$ m) on the *X-Z* plane, as shown in Fig. 3(b).

3.2. System properties and initial conditions

The hydraulic and thermal properties of the reservoir system used in this simulation, as well as the initial conditions, are obtained from the field measurements at the AT1 test site and reasonable predications [7,12,21,35], and are summarized in Table 1. In this study, in order to simplify the geologic system and improve computational efficiency, the porosity, absolute permeability, and initial hydrate saturation are assumed to be uniformly distributed in each zone (OB, HBL-1, HBL-2, HBL-3, and UB), and are calculated by averaging the layer values in Fig. 2 into the multi-layered model. Previous studies [20,24] indicated that layered structure of reservoir (e.g. HBL-1 is composed of thin alternations of sand and silt layers) can lead to the anisotropy of permeability ($k_v < k_h$, k_v is the vertical permeability, and k_h is horizontal permeability). Therefore, the permeability anisotropy of HBL is considered in this numerical

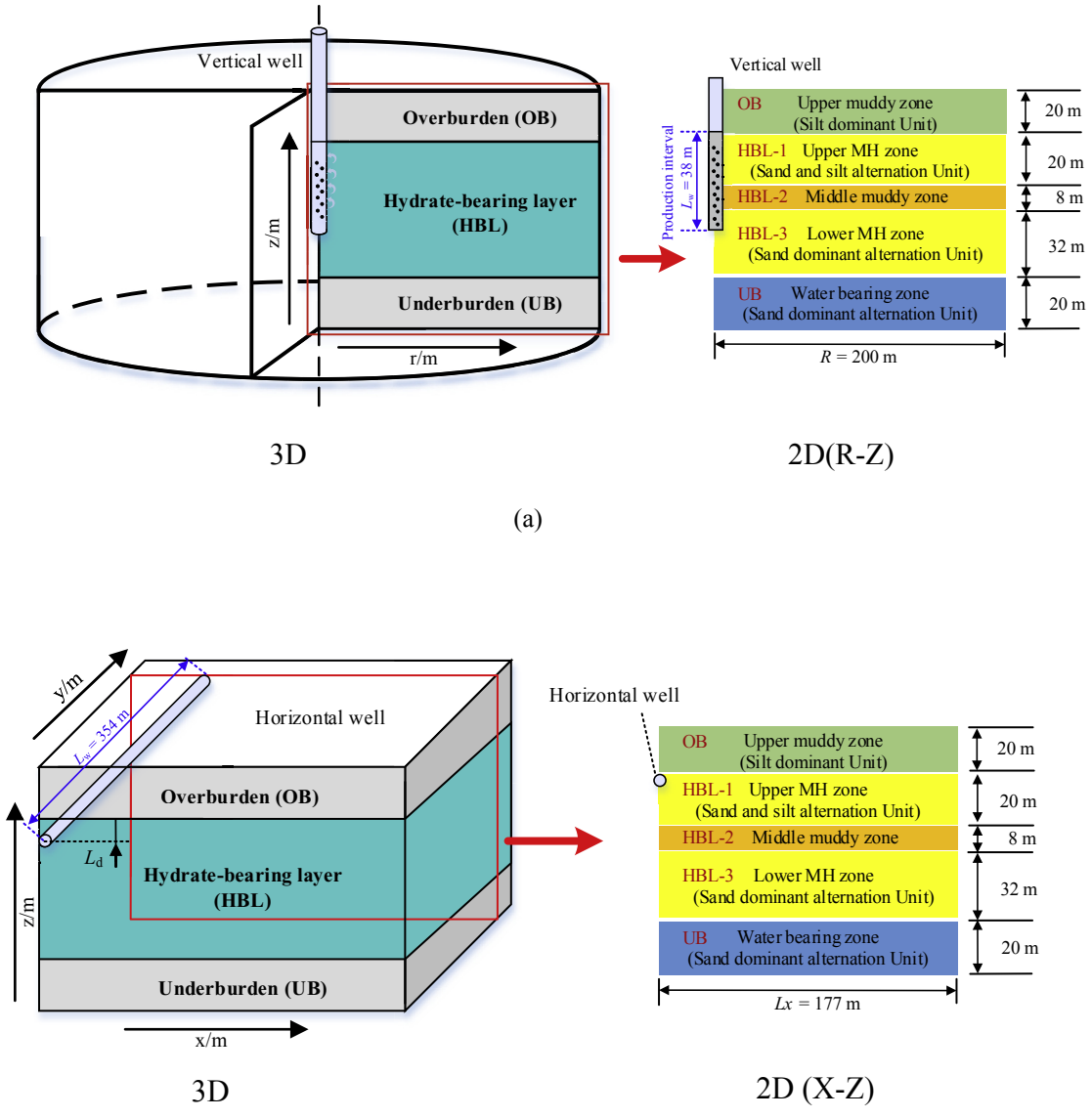

Fig. 3. System geometries and configurations of (a) the single vertical well producing from a cylindrical section and (b) the horizontal well producing from a rectangular section of the hydrate reservoir.

Table 1
Main properties of the layered hydrate reservoir and initial conditions.

Parameter	Value	Parameter	Value
HBL-1 thickness H_1	20 m	Initial saturation $S_{H\text{-}3}$ in HBL-3	0.6
HBL-2 thickness H_2	8 m	Permeability k_V, k_H in HBL-1	0.3D, 0.2D
HBL-3 thickness H_3	32 m	Permeability k_V, k_H in HBL-2	0.05D, 0.05D
Initial p_0 at base of HBL-3	13.4 MPa	Permeability k_V, k_H in HBL-3	0.4D, 0.3D
Initial T_0 at base of HBL-3	14.8 °C	Permeability k_{OB} in OB	0.01D
Porosity ϕ in the HBL	0.40	Permeability k_{UB} in UB	1.0D
Initial saturation $S_{H\text{-}1}$ in HBL-1	0.5	Well pressure p_w	3.0 MPa
Initial saturation $S_{H\text{-}2}$ in HBL-2	0.35	Well temperature T_w	1.0 °C

study, as shown in Table 1.

In both the cylindrical and the rectangular systems, the initial pressure and temperature distributions are referred from the well logging data [7], as shown in Fig. 4. During the numerical simulation, constant pressure and temperature conditions are applied at the uppermost and lowermost boundaries of the simulated region, and no mass and heat flow conditions are applied at the other two boundaries except the production interval. To avoid a

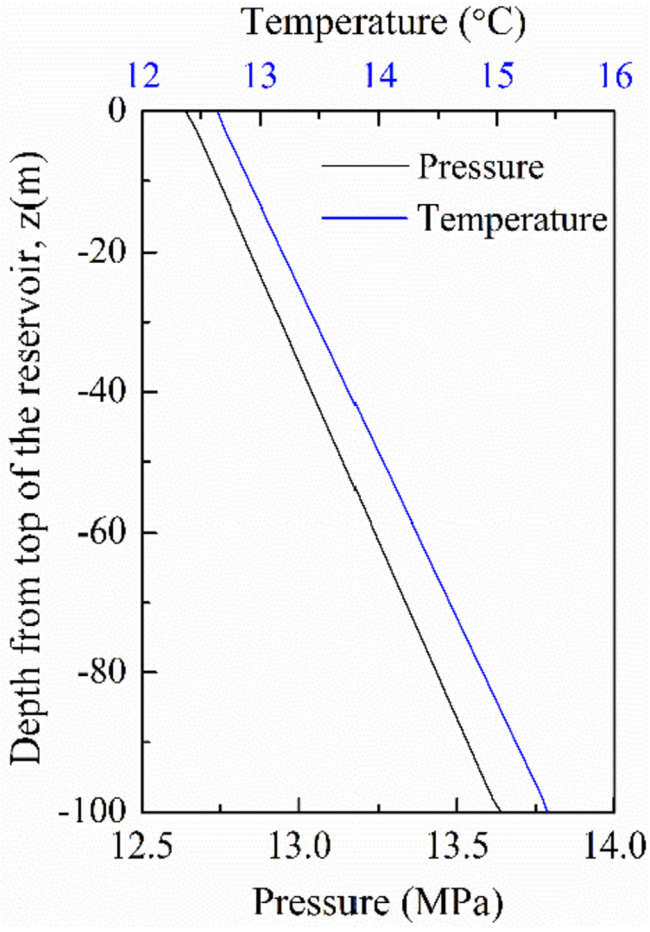

Fig. 4. Initial pressure and temperature distributions with system depth.

theoretically correct but computationally intensive solution of the Naiver-Stokes equation [9], the well is represented as pseudo-porous media with porosity $\phi = 1.0$, permeability $k = 10^{-8}$ D, and capillary pressure $p_{cap} = 0$ Pa.

3.3. Simulation approach

In this study, we used Tough + Hydrate (T + H) code to conduct the numerical simulation. This code is a member of the TOUGH + family developed by the Lawrence Berkeley National Laboratory, and is able to deal with multiphase and multicomponent problems related to the system response of common natural methane hydrate deposits, including the non-isothermal hydration reactions, phase behavior, and heat and mass transfer in complex geologic media. This code has been proved with good reliability and validity in the simulation of methane hydrate dissociation and formation [36–38], and is now widely used in the analysis and prediction of gas production from hydrate-bearing systems at different scales (core-scale, pilot-scale and reservoir-scale). The detailed theories related to the T + H code are described in Ref. [39].

4. Results and discussions

In this section, the gas production performances from the multi-layered reservoir using a single vertical and a single horizontal wells are investigated, respectively. Depressurization method is applied to induce dissociation during gas production. In order to validate the constructed reservoir model and the numerical code, the well pressure in the first 6 days of gas production is the same ($p_w = 5.0$ MPa in the first 4 days, and $p_w = 4.3$ MPa in the subsequent 2 days) to the field test data [7], and then is reduced to 3.0 MPa after 10 days of gas production. In addition, the sensitivity of gas production using horizontal well to the system parameters of MH reservoir is analysed.

4.1. The case of production using a vertical well

4.1.1. Comparison with the 2013 offshore production test in Japan

Fig. 5 shows the comparison of the volumetric rates of the produced gas Q_G and water Q_W at the well between our work and the field test data in the Eastern Nankai Trough in 2013. It can be observed from Fig. 5 that the simulated Q_G matches well with the field observation during the 6-day production period. The average Q_G in numerical simulation is approximately 19,575 ST m^3/d, which is very close to the field test data (20,000 ST m^3/d). But for Q_W, a certain deviation is identified between the numerical simulation and field test data. This phenomena also occurred in the simulation work [35]. The reason can be explained by the reservoir disturbance in the initial production because of drilling and gravel packing operations and the lateral reservoir heterogeneity in practical production test. For numerical simulation, it is difficult to reproduce these short-term behaviours in practical production test with very accurate values. But in general, the numerical result is basically consistent with the field test data, which proves the reasonability and reliability of the numerical code and the constructed model in this study. The following simulation work is conducted based on this constructed model.

4.1.2. Long-term behavior of gas and water production

Fig. 6 shows the evolution of the volumetric rate of produced gas (Q_G) at the well, the cumulative volumes of produced gas (V_G) and free gas remaining in the reservoir (V_F) during long-term production by the vertical well. The evolution of Q_G is characterized by a rapid increase in the initial short period (stage 1, to t = 10 days), succeeded by a medium period of rapid decline (stage 2) that lasts for approximately 200 days, and followed by a long period of continuous but mild decline (stage 3), which is very similar to the observations in the experimental and numerical studies of gas production from sand-dominant MH accumulations [14,17,40]. At the end of stage 1, Q_G reaches its peak value (3.6×10^4 ST m^3/d). After continuous production of $t = 1390$ days, a total of $V_G = 1.35 \times 10^7$ ST m^3 gas is produced at the vertical well, most of

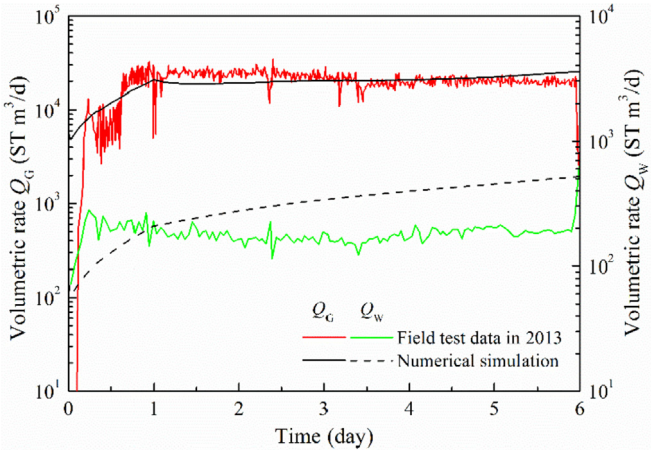

Fig. 5. Comparison of volumetric rates of produced gas (Q_G) and water (Q_W) at the well between the numerical results and the field test data in 2013 [7].

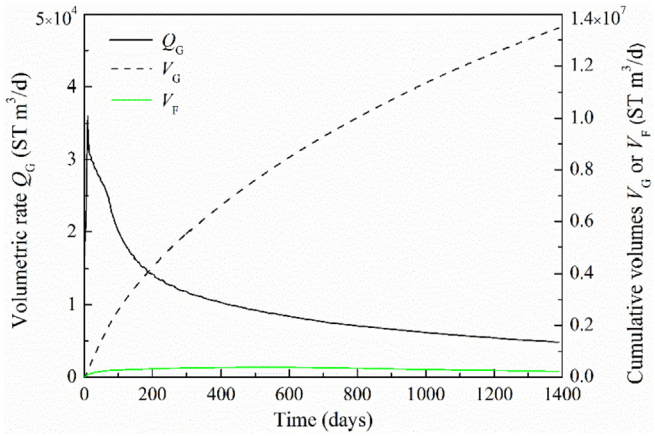

Fig. 6. Evolution of the volumetric rate of produced gas (Q_G) at the well and the cumulative volumes of produced gas (V_G) and free gas remaining in the reservoir (V_F) during long-term production for the vertical well case.

which is produced at stage 3. The average Q_G is 9.69×10^3 ST m^3/d. However in commercial natural gas production, the requirement of gas production rate is 3.0×10^5 ST m^3/d [41]. Therefore, the gas production performance from such multi-layered hydrate reservoir using the vertical well is insufficient for gas production in industry level. The free gas V_F remains at low levels during the entire production period, indicating that most of the gas released from dissociation is produced at the vertical well.

Fig. 7 shows the evolution of the volumetric rate of produced water (Q_W) at the well and the gas-to-water ratio (R_{GW}) during long-term production by the vertical well. During the production period except for the initial short stage, the produced water V_W increases almost linearly with time, indicating a relatively stable water production rate. At the end of continuous production, a total of $V_W = 1.43 \times 10^7$ m^3 water is produced at the vertical well. R_{GW} is regarded as a relative criterion for evaluating the production performance and is computed as $R_{GW} = V_G/V_W$. A higher R_{GW} means a relatively low cost on drawing water from well and a high energy efficiency during production operation. As shown in Fig. 8, R_{GW} shows a rapid decline in the initial period ($t < 100$ days), followed by a long-term but gradual decline. This can be attributed to the continuous decrease of Q_G in stage 1 and stage 2 (as shown in Fig. 6). In addition, it is found that R_{GW} maintains low levels ($0.9 < R_{GW} < 2$) after $t = 519$ days.

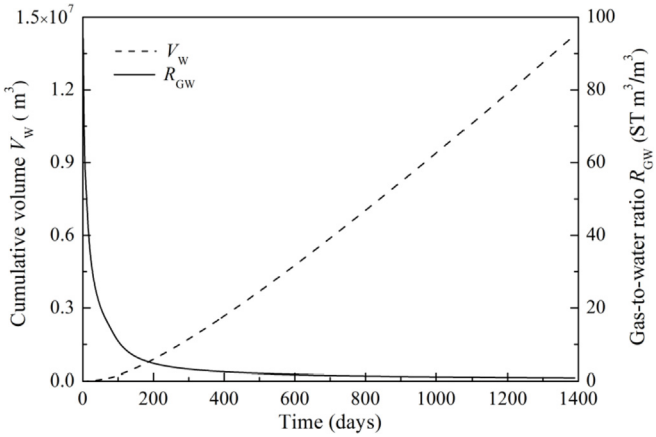

Fig. 7. Evolution of the cumulative volume of produced water (Q_W) at the well and the gas-to-water ratio (R_{GW}) during long-term production for the vertical well case.

4.1.3. Spatial distributions during long-term production

Fig. 8 shows the spatial distributions of temperature (T), hydrate saturation (S_H), and gas saturation (S_G) on days 6 and 1095 during the long-term production by the vertical well. White lines in Fig. 8 indicate the initial boundaries of HBL-1, HBL-2, and HBL-3. At $t = 6$ days, a low-temperature region is identified in the vicinity of the production well, which is related to endothermic reaction of hydrate dissociation. The hydrate within a few meters from the well has completely dissociated. In addition, it is found that the hydrate dissociation zone expands beyond the production interval in vertical direction. Note that the originating undissociated hydrate between the production interval and the water-bearing zone play an important role as self-sealing layer that prevent water in the water-bearing zone from flowing into the HBL and the production well, and ensure the depressurization effect. The released gas mainly accumulates in the hydrate-free zone. The higher S_G in HBL-2 is caused by the low permeability, which severely reduces the mobility of gas and water. However at $t = 1095$ days, the hydrate below the production interval has completely dissociated, meaning that the hydrate self-sealing effect disappears. Therefore, a large amount of water from the water-bearing zone flows into the HBL and the depressurization effect is significantly weakened, which can be further confirmed by the high-temperature zone in temperature distribution and the low Q_G levels of Fig. 6.

From the analysis above, the low gas production rate Q_G and gas-to-water ratio R_{GW} are the major bottlenecks for long-term gas production from such multi-layered MH reservoirs when using the vertical well. Compared to the vertical well, the horizontal well can reach more reservoir domain, which would induce more hydrate to be dissociated. Thus, in this study, a single horizontal well is employing to conduct the gas production with the hope of enhancing the gas production performance. In the following sections, we investigate the gas production performance by the horizontal well, as well as the factors affecting it.

4.2. The case of production using a single horizontal well

4.2.1. Gas production

Fig. 9 shows the evolution of Q_G from the horizontal well during long-term production, and includes for the vertical well case for comparison. It is clear from the comparison of Q_G that the use of horizontal well shows a better production performance over the vertical well. For $t < 700$ days, the evolution of Q_G in the vertical and horizontal well cases follows the similar trend: increase sharply in the initial short stage ($t < 10$ days), which may be attributed to the expansion of hydrate dissociation zone and high pressure difference Δp between the well pressure and the pressure at the dissociation front, and then decrease gradually for a long period due to the continuously diminishing driving force Δp. During this period, Q_G in the horizontal well case is about one order of magnitude larger than the one corresponding to the vertical case. After that time, Q_G of the horizontal well shows some fluctuations with a rapidly declining trend, which can be attributed to the instantaneous change of temperature and pressure on the dissociation front because of the endothermic reaction and the complex multiphase flow after the destruction of self-sealing layer, and the difference value between the two curves gets smaller gradually. At approximately $t = 1410$ days, Q_G in the horizontal well case drops sharply to zero, and no gas is produced after this time.

Fig. 10 shows the evolution of V_G and V_F during the long-term gas production by horizontal well, and includes for the vertical well case for comparison. By comparing these two cases, it is found that both V_G and V_F of the horizontal well case are about one order of magnitude larger than the ones corresponding to the vertical well case. This greatly proves the higher performance of horizontal

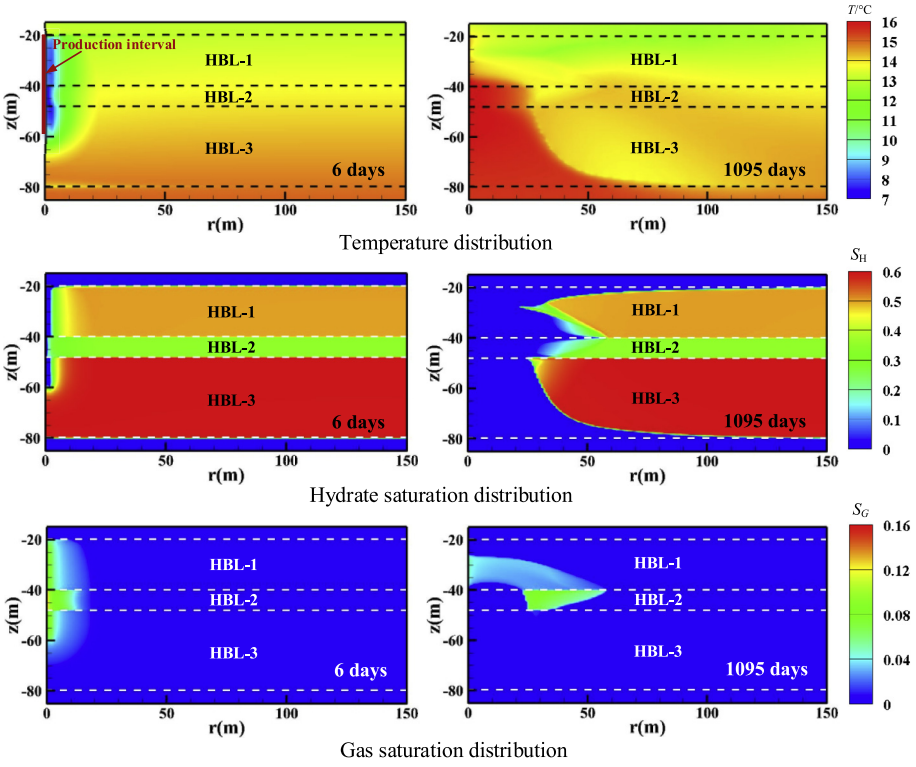

Fig. 8. Spatial distributions of temperature (T), hydrate saturation (S_H), and gas saturation (S_G) on days 6 and 1095 during long-term production for the vertical well case.

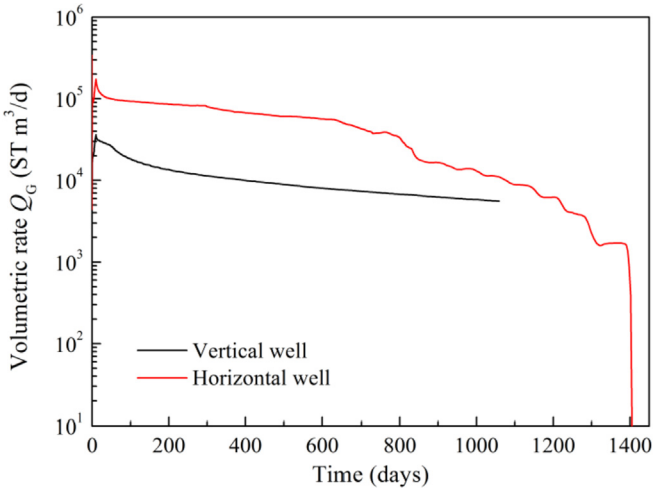

Fig. 9. Comparison of Q_G between the vertical and horizontal well cases during long-term gas production.

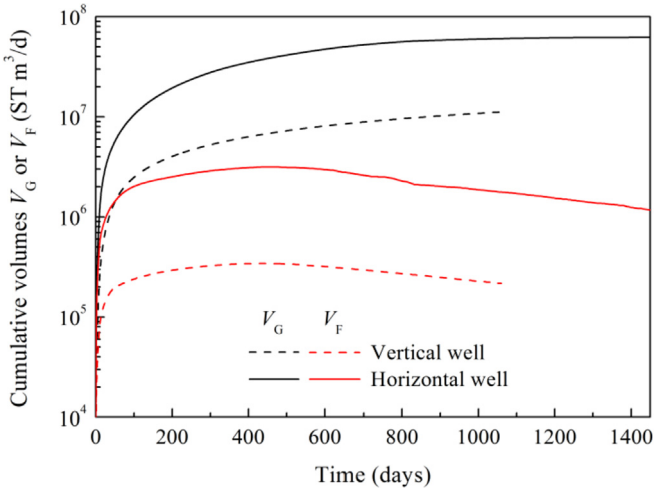

Fig. 10. Comparison of V_G and V_F between the vertical and horizontal well cases during long-term gas production.

well. Other than these, more information of gas production using vertical and horizontal wells in a two-year production period is listed in Table 2. It is observed that the use of horizontal well shows high average Q_G, which is 7.3×10^4 ST m^3/d. This value significantly exceeds the production test data at the Nankai Trough in 2013 (approximately 2.0×10^4 ST m^3/d) [7] and at the South China Sea in 2017 (approximately 5.0×10^3 ST m^3/d) [26]. After continuous production for two years, 25.4% of the hydrate existed in the reservoir model has been released, which is approximately 6 times higher than the evaluation of the gas production using vertical well. During the entire period, the remaining free gas V_F is very smaller in comparison to the corresponding gas production V_G. This confirms that most of the gas released from dissociation is produced at the horizontal well, which is also identified in the vertical well case.

Table 2
Comparison of the production performances between the vertical and horizontal well cases in the initial two years.

Simulated result	Vertical well	Horizontal well
V_G (ST m^3)	9.5×10^6	5.4×10^7
Average Q_G (ST m^3/d)	1.3×10^4	7.3×10^4
Recovery factor (%)	4.8	25.4

It is clear from the above comparison that the use of horizontal

well appears to be more effective for extracting gas from such multi-layered reservoirs. While the average Q_G is still lower than the requirement of commercial production (3.0×10^5 ST m^3/d), it is possible that the gas production performance can be further improved with the longer horizontal well, different well configurations, and more complex production strategies.

4.2.2. Water production

Fig. 11 shows the comparison of V_W and R_{GW} between the horizontal and vertical well cases during long-term gas production. For both cases, V_W increases slowly in the early stage. This stage is associated with the hydrate dissociation. However, as the production processes, V_W increases linearly with a high water production rate in the later production stage. This can be attributed to the destruction of self-sealing layer (the hydrate between the horizontal well and the water-bearing zone), leading to a large amount of water from the water-bearing zone flowing into the HBL. During the entire production, V_W is slightly lower in the horizontal well case, and a total of $V_W = 9.78 \times 10^6$ m^3 water is produced at the end of production. In addition, it is clear in Fig. 11 that both the R_{GW} curves show a decline trend from the initiation, and the average R_{GW} during the entire production period are 0.9 and 6.3 for the vertical and horizontal well cases, respectively. This suggests that the horizontal well has a better production performance over the vertical well in the relative criterion. But in general, the gas-to-water ratio for both cases is low in absolute terms, considering the energy efficiency and economic efficiency. On the other hand, high water production in the later production stage would increase the possibility of sand production for real gas production. Thus water management is an important aspect that should be considered in the design and analysis of long-term gas production from such multi-layered reservoirs by depressurization no matter which type of production well (horizontal well or vertical well) is employed.

4.2.3. Spatial distributions

Fig. 12 shows the evolution of temperature distribution (T) during long-term gas production by the horizontal well. In the initial production stage ($t = 30$ days), a significant temperature drop is identified around the production well, which is associated the strong endothermic reaction of hydrate dissociation. Meanwhile, another low-temperature zone is observed along the bottom of HBL-3, indicating hydrate dissociation in this region. This dissociation reaction is mainly caused by the continuing geothermal heat inflows from the water-bearing zone. But thereafter ($t = 180$–365 days), the temperature near the production well gradually increases, which can be attributed to the surrounding heat flow, and the low-temperature zone along the bottom of HBL-3 continues to expand upward and horizontally. Since $t = 730$ days, an expanding high-temperature zone is identified below the horizontal well, which is across the HBL-1, HBL-2 and HBL-3. This phenomenon indicates that the high-temperature water in the water-bearing zone flows into the HBL and the production well, which is consistent with the high rate of water production in the later production period seen in Fig. 11.

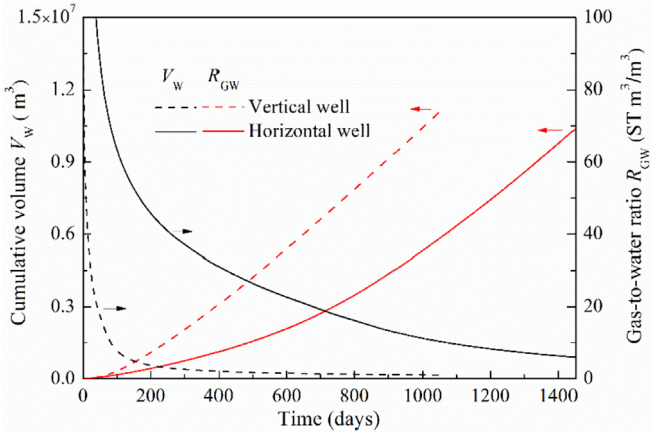

Fig. 11. Comparison of Q_W and R_{GW} between the vertical and horizontal well cases during long-term production.

Fig. 13 shows the evolution of the hydrate saturation (S_H) distribution during long-term gas production by the horizontal well. In the initial production stage ($t = 30$ days), a hydrate-free zone is identified around the well, and hydrate dissociation occurs mainly within the HBL-1 and expands horizontally because of the high horizontal permeability of HBL-1 and the proximity to the horizontal well. As time passes, the hydrate dissociation zone expands across the HBL-2 and towards the HBL-3, and another hydrate-free zone emerges at the bottom of HBL-3, and expands upwards and horizontally, which indicates hydrate dissociation in this region. This is consistent with the low-temperature zone in temperature distribution (as shown in Fig. 12, $t = 180$ days). However after $t = 730$ days, it is observed that the hydrate between the horizontal well and the water-bearing zone (serves as the self-sealing layer) has completely dissociated, and hydrate dissociation front in the entire HBL advances slowly. This can be attributed to the weakening depressurization effect after the destruction of self-sealing layer. Meanwhile, a small hydrate reformation zone (higher S_H) is identified along the advanced front of the dissociation zone in the HBL-1. Moreover, it is found that the dissociation front in the HBL-2 advances more quickly compared with those in HBL-1 and HBL-3 during the entire production period. This is association with the low hydrate saturation in HBL-2.

Fig. 14 shows the evolution of the gas saturation (S_G) distribution during long-term gas production by the horizontal well. It is observed from Fig. 14 that most of the free gas accumulates in the HBL-1 and HBL-2 during the entire production period. This is caused by the low vertical permeability of HBL-1 and HBL-2 and the buoyancy of the gas released from dissociation. In addition, the free-gas zone below the horizontal well completely disappears after $t = 730$ days. A comparison of the T and S_G profiles in Figs. 12 and 14 indicates that the free-gas zone below the horizontal well is occupied by the high-temperature water inflows from the water-bearing zone. Therefore, the free-gas zone shrinks in the later production stage, meaning the decrease of the cumulative volume of free gas. This is consistent with the appearance of the V_F curve in Fig. 10.

4.3. Sensitivity analysis

In this section, we investigate the sensitivity of gas production by the horizontal well to the following system parameters: The permeability k_2 of HBL-2, the permeability anisotropy of HBL-1 and HBL-3, and the initial saturation S_H of HBL-3.

4.3.1. Sensitivity to the permeability k_2 of HBL-2

Since HBL-2 locates between HBL-1 and HBL-3, the permeability of HBL-2 is sure to affect the expansion of depressurization effect and hydrate dissociation in entire HBL, which may ultimately affect the gas production behavior from the multi-layered reservoir. Fig. 15 shows the evolution of V_G and R_{GW} for different permeability k_2 of HBL-2. As shown in Fig. 15, decreasing k_2 from 50 mD to 10 mD results in significant decline of V_G. This can be attributed to the unfavorable condition for fluids flow between HBL-1 and HBL-3 that significantly limits the dissociation reaction in HBL-3. The

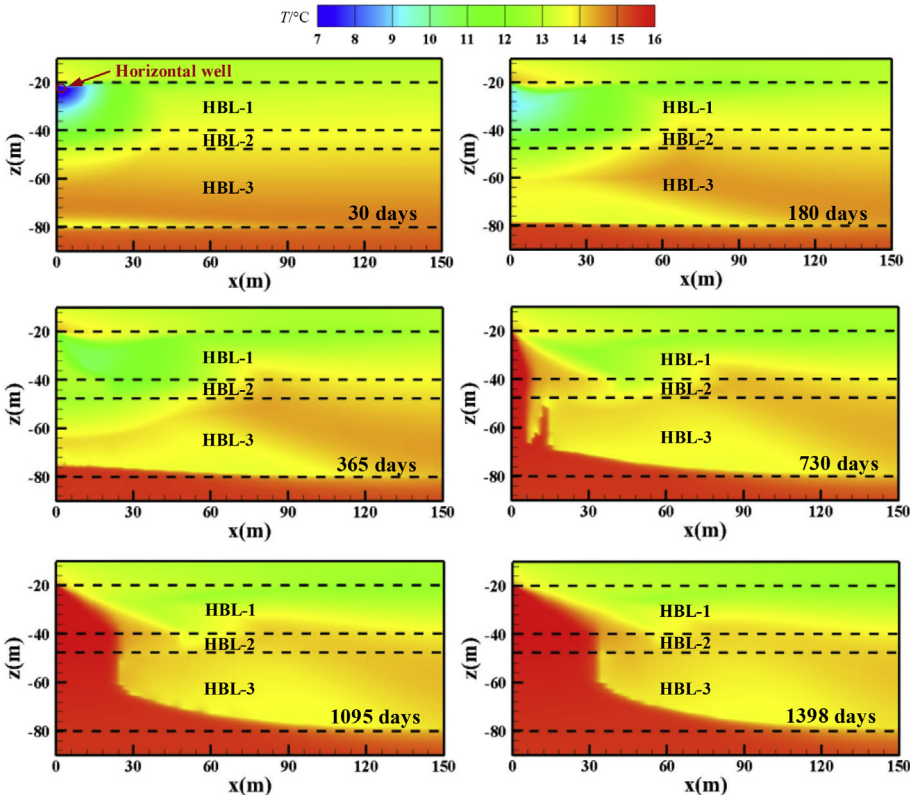

Fig. 12. Evolution of the temperature (T) distribution in the reservoir during long-term production for the horizontal well case.

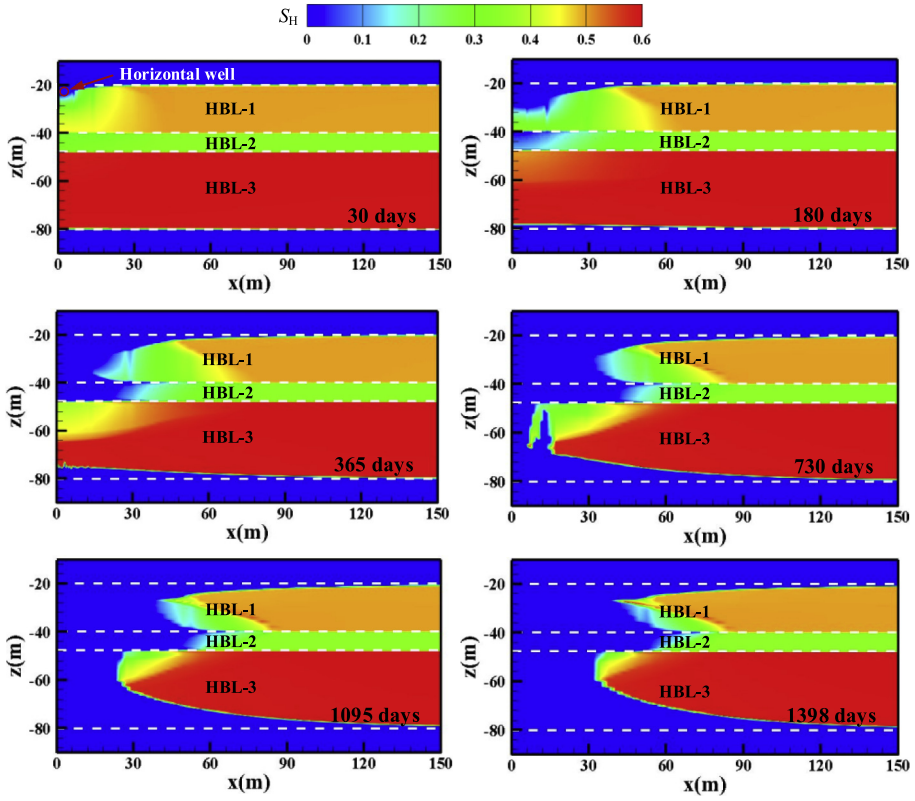

Fig. 13. Evolution of the hydrate saturation (S_H) in the reservoir during long-term production for the horizontal well case.

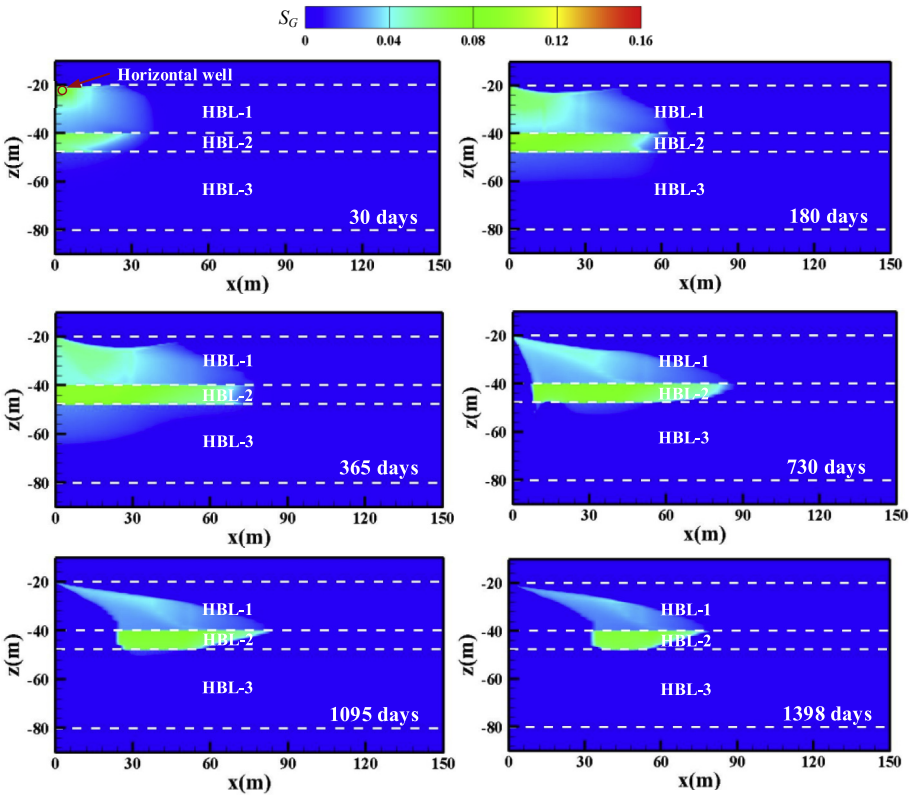

Fig. 14. Evolution of the gas saturation (S_G) in the reservoir during long-term production for the horizontal well case.

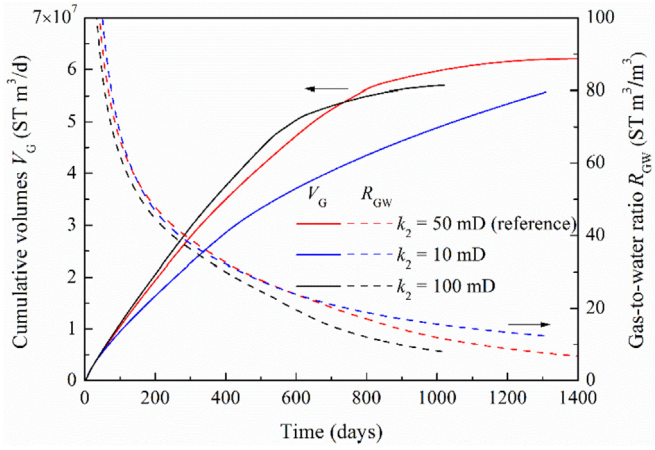

Fig. 15. Sensitivity of V_G and R_{GW} to the permeability k_2 of HBL-2.

weaker hydrate dissociation in HBL-3 is further demonstrated by the comparison of hydrate saturation distributions in Fig. 16, which shows smaller hydrate-free zone for the lower k_2 case. For this reason, the water flow from the water-bearing zone to the production well is supressed effectively, which leads to higher R_{GW} levels in the later production stage. However, when increasing k_2 from 50 mD to 100 mD, V_G increases at a higher rate (higher Q_G) for a long production period because of strong hydrate dissociation in HBL-3, but the pattern reverses at the later production stage ($t > 600$ days). This is because an increase of k_2 leads to an earlier destruction of the self-sealing layer in HBL-3, which will weaken the depressurization effect and results in a higher water production (V_W). Thus, the case of $k_2 = 100$ mD has the lower R_{GW} during the entire production period. From the above analysis, it is clear that the permeability k_2 of HBL-2 has a strong effect on gas production from such multi-layered hydrate reservoirs, and both the very higher and lower levels of k_2 are unfavorable for long-term gas production.

4.3.2. Sensitivity to the permeability anisotropy of HBL-1 and HBL-3

As described in Section 3, HBL-1 and HBL-3 have high permeability and moderate hydrate saturation, and thus are the main targets for gas production. In addition, the HBL-1 is composed of thin alternations of sand and silt layers, and HBL-3 is composed of relatively thick sand-dominant sequences. This layer structure can lead to the permeability anisotropy (the vertical permeability k_V is lower than the horizontal permeability k_H) of HBL-1 and HBL-3. In this study, two cases (shown in Table 3) with different vertical permeability are considered to investigate the effect of permeability anisotropy on gas production performance. Fig. 17 shows the evolution of V_G and R_{GW} for these three cases. It is clear from Fig. 17 that the decrease in vertical permeability extends the production period, but has less effect on the final gas production V_G and gas-to-water ratio R_{GW}. This means that the lower vertical permeability case has a lower gas production rate (Q_G). This can be explained by the fact that: (1) The lower vertical permeability limits the vertical expansion of the dissociation zone and fluids flow within the sub-HBLs, and thus results in a lower gas production rate (Q_G); (2) The lower vertical permeability delays the time of destruction of the self-sealing layer in HBL-3, and thus extends the gas production period. The strong effect of the vertical permeability on gas production is also demonstrated by the comparison of hydrate saturation distributions in Fig. 18, which shows that the dissociation zone in the lower permeability case propagates more slowly. From the above analysis, it is determined that the permeability

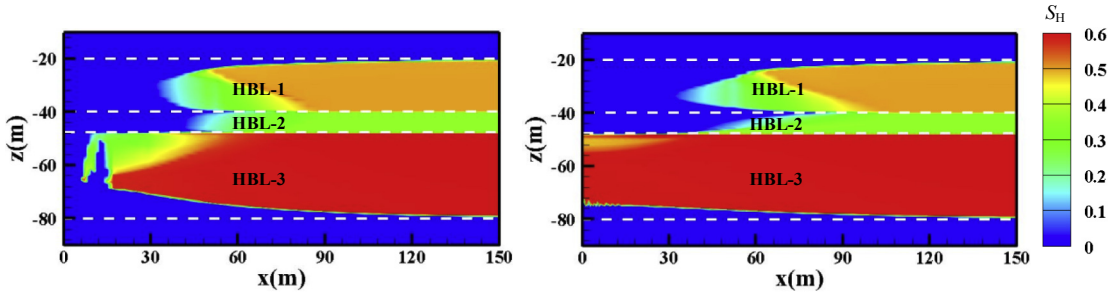

(a) k_2 = 50 mD (b) k_2 = 10 mD

Fig. 16. Hydrate saturation (S_H) in the reservoir on day 730 for (a) $k_2 = 50$ mD and (b) $k_2 = 10$ mD cases.

Table 3
The cases of permeability anisotropy in numerical simulation.

Case	HBL-1 ($k_V = 0.4$ D)	HBL-2 ($k_V = 0.3$ D)
Reference case	$k_H = 0.3$ D	$k_H = 0.2$ D
Case1	$k_H = 0.4$ D	$k_H = 0.3$ D
Case2	$k_H = 0.2$ D	$k_H = 0.1$ D

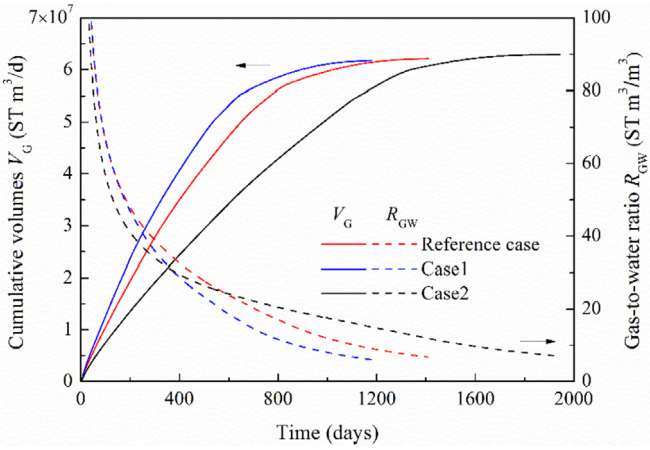

Fig. 17. Sensitivity of V_G and R_{GW} to the permeability anisotropy of HBL-1 and HBL-3.

anisotropy is a key factor affecting long-term gas production from such multi-layered reservoirs, and lower vertical permeability will significantly reduce gas production efficiency. Therefore, it will be more favorable for gas production from the multi-layered reservoir with more sand layers and less silt layers (higher vertical permeability).

4.3.3. Sensitivity to the initial hydrate saturation $S_{H\text{-}3}$ of HBL-3

As described in Section 3, the thickness of HBL-3 is considerably larger than that of HBL-1. Therefore, the hydrate saturation $S_{H\text{-}3}$ of HBL-3 is a key factor affecting the production potential of this MH reservoir. Fig. 19 shows the effect of initial hydrate saturation $S_{H\text{-}3}$ of HBL-3 on gas production. It is clear from Fig. 19 that decreasing $S_{H\text{-}3}$ from 0.6 to 0.5 leads to slightly higher gas production V_P and lower R_{GW} in the initial stage, but the effect on V_P is reversed in the later stage. The higher V_P in the early stage can be attributed to the higher effective permeability of HBL-3 that corresponds to lower $S_{H\text{-}3}$ levels for a giving porosity. On the other hand, the higher effective permeability of HBL-3 results in an earlier destruction of the self-sealing layer, which is unfavorable for the expansion of depressurization effect and significantly promote water production. However, when increasing $S_{H\text{-}3}$ from 0.6 to 0.7, the gas production V_F shows significant decline in a long period of gas production, but finally converges to the same level, and the R_{GW} shows slight increment in the later stage. The lower V_F in the early stage is attributed to the lower effective permeability of HBL-3. On the other hand, the local effective permeability of HBL-3 increases gradually with hydrate dissociation, and for the higher $S_{H\text{-}3}$ case, more hydrate can be potentially exploited from the reservoir, both which result in higher gas production rate in the later production period. From the above analysis, it is determined that both the very higher and lower levels of $S_{H\text{-}3}$ are unfavorable for long-term gas production, which is similar to the effect of the permeability k_2 of HBL-2.

5. Conclusions

In this study, we numerically investigated gas production from a multi-layered hydrate reservoir by depressurization with a single vertical well and a single horizontal well, respectively, and the sensitivity of gas production using horizontal well to the main system parameters was also analysed. Based on the numerical results of this study, the following conclusions are drawn:

a. A multi-layered MH reservoir model is constructed based on the logging and pressure core data at the AT1 site located in the Eastern Nankai Trough, Japan. Through comparison with the recorded field test data during short-term production, the numerical code and the constructed model is proved to be reasonable and reliable in predicting the hydrate dissociation behavior in the Eastern Nankai Trough.
b. When using the vertical well, the average gas production rate Q_G during long-term gas production is 9.69×10^3 ST m^3/d, and cannot satisfy the industry production requirement of 3.0×10^5 ST m^3/d. In addition, the gas-to-water ratio R_{GW} remains at low levels ($0.9 < R_{GW} < 2$) for a long production period.
c. Compared with the vertical well, the horizontal well has better gas production performance in the absolute criterion (Q_G) and relative criterion (R_{GW}). Over a production period of two years, the average Q_G by using the horizontal well reaches 7.3×10^4 ST m^3/d, which is 5.7 times higher than that by using the vertical well. Moreover, it is possible that the gas production performance can be further enhanced to attain commercially viable performance with the longer horizontal well, different well configurations, and more complex production strategies.
d. No matter which type of production well (horizontal well or vertical well) is employed, the gas-to-water ratio R_{GW} during long-term gas production is low in absolute terms. This is

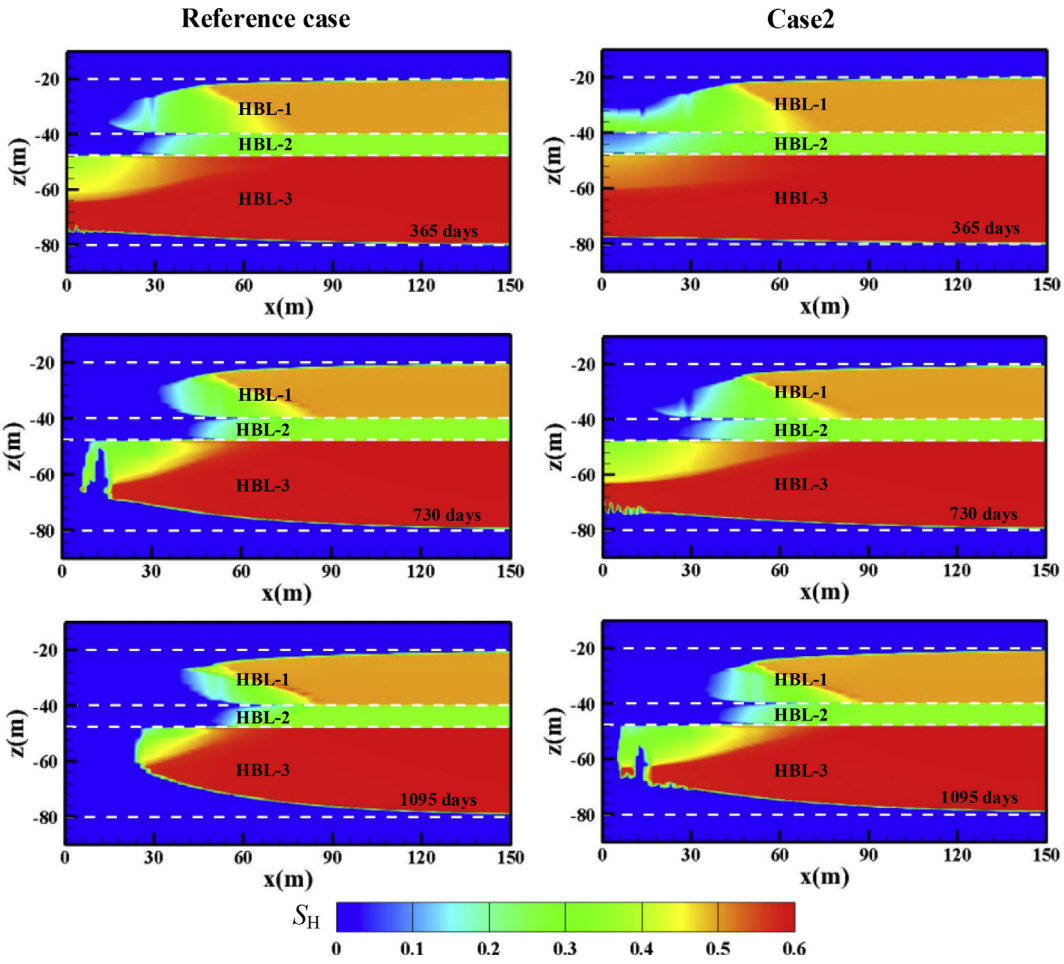

Fig. 18. Effect of the permeability anisotropy of HBL-1 and HBL-3 on the evolution of hydrate saturation (S_H) in the reservoir.

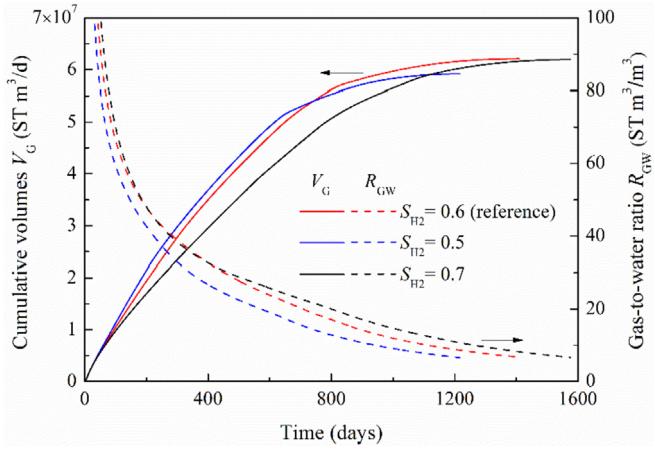

Fig. 19. Sensitivity of V_G and R_{GW} to the initial hydrate saturation S_{H-3} of HBL-3.

associated with the relatively large amount of produced water caused by the water inflows from the water-bearing zone. Therefore, more attention should be paid to water management in the development of such multi-layered reservoirs by depressurization.

e. The sensitivity analysis indicates that the permeability k_2 of HBL-2 and the initial hydrate saturation S_{H-3} of HBL-3 have a strong effect on the gas production from such multi-layered hydrate reservoirs when using the horizontal well, and both the very higher and lower levels of k_2 and S_{H-3} are unfavorable for long-term gas production.

f The permeability anisotropy of HBL-1 and HBL-3 has less effect on the final gas production V_F and gas-to-water ratio R_{GW} when using the horizontal well, but has a greater effect on the gas production efficiency. A decreasing vertical permeability can lead to obvious decline of gas production rate as it provides an adverse condition for fluids flow in the vertical direction. Therefore, it will be more favorable for gas production from the multi-layered hydrate reservoir with more sand layers and less silt layers (higher vertical permeability).

The findings of this study provide a reference for the analysis and future commercial production targeting such Nankai Trough reservoirs. In addition, the gas production from a more refined multi-layered reservoir will be further investigated in the future work.

Acknowledgments

The support from JST-CREST Project (No. JPMJCR13C4: Breakthrough on multi-scale interfacial transport phenomena in oceanic methane hydrate reservoir and application to large-scale methane production) is gratefully acknowledged by the authors.

Nomenclature

k	absolute permeability (D)
k_H	absolute permeability in horizontal direction (D)
k_V	absolute permeability in vertical direction (D)
L_d	distance between horizontal well and overburden (m)
L_w	length of production interval (m)
p	pressure (MPa)
Q_G	volumetric rate of produced gas at production well (ST m^3/day)
R_{GW}	ratio of gas to water production (ST m^3 of CH_4/m^3 of H_2O)
S	phase saturation
t	time (day)
T	temperature (°C)
V_F	cumulative volume of free gas remaining in reservoir (ST m^3)
V_G	cumulative volume of produced gas at production well (ST m^3)
V_W	cumulative volume of produced water at production well (m^3)

Greek symbols

ϕ	porosity

Superscripts and subscripts

0	denotes initial state
F	free gas
H	hydrate phase
G	gas phase
OB	overburden
UB	underburden

References

[1] Sloan ED. Fundamental principles and applications of natural gas hydrates. Nature 2003;426(6964):353–63.
[2] Milkov AV. Global estimates of hydrate-bound gas in marine sediments: how much is really out there? Earth Sci Rev 2004;66(3–4):183–97.
[3] Collett T, Bahk J-J, Baker R, Boswell R, Divins D, Frye M, et al. Methane hydrates in nature—current knowledge and challenges. J Chem Eng Data 2015;60(2):319–29.
[4] Boswell R, Yamamoto K, Lee S-R, Collett T, Kumar P, Dallimore S. Chapter 8 - methane hydrates. In: Letcher TM, editor. Future energy. second ed. Boston: Elsevier; 2014. p. 159–78.
[5] Maruyama S, Deguchi K, Chisaki M, Okajima J, Komiya A, Shirakashi R. Proposal for a low CO2 emission power generation system utilizing oceanic methane hydrate. Energy 2012;47(1):340–7.
[6] Yamamoto K, Terao Y, Fujii T, Ikawa T, Seki M, Matsuzawa M, et al. Operational overview of the first offshore production test of methane hydrates in the Eastern Nankai Trough. Offshore technology conference. Houston, Texas: Offshore Technology Conference; 2014.
[7] Konno Y, Fujii T, Sato A, Akamine K, Naiki M, Masuda Y, et al. Key findings of the world's first offshore methane hydrate production test off the coast of Japan: toward future commercial production. Energy Fuels 2017;31(3):2607–16.
[8] Konno Y, Masuda Y, Hariguchi Y, Kurihara M, Ouchi H. Key factors for depressurization-induced gas production from oceanic methane hydrates. Energy Fuels 2010;24(3):1736–44.
[9] Moridis GJ, Silpngarmlert S, Reagan MT, Collett T, Zhang K. Gas production from a cold, stratigraphically-bounded gas hydrate deposit at the mount elbert gas hydrate stratigraphic test well, Alaska north slope: implications of uncertainties. Mar Petrol Geol 2011;28(2):517–34.
[10] Konno Y, Oyama H, Nagao J, Masuda Y, Kurihara M. Numerical analysis of the dissociation experiment of naturally occurring gas hydrate in sediment cores obtained at the eastern Nankai Trough, Japan. Energy Fuels 2010;24(12):6353–8.
[11] Konno Y, Uchiumi T, Oyama H, Jin Y, Nagao J, Masuda Y, et al. Dissociation behavior of methane hydrate in sandy porous media below the quadruple point. Energy Fuels 2012;26(7):4310–20.
[12] Konno Y, Yoneda J, Egawa K, Ito T, Jin Y, Kida M, et al. Permeability of sediment cores from methane hydrate deposit in the Eastern Nankai Trough. Mar Petrol Geol 2015;66:487–95.
[13] Li B, Li G, Li XS, Li QP, Yang B, Zhang Y, et al. Gas production from methane hydrate in a pilot-scale hydrate simulator using the huff and puff method by experimental and numerical studies. Energy and Fuels 2012;26(12):7183–94.
[14] Li G, Li B, Li XS, Zhang Y, Wang Y. Experimental and numerical studies on gas production from methane hydrate in porous media by depressurization in pilot-scale hydrate simulator. Energy and Fuels 2012;26(10):6300–10.
[15] Li X-S, Wang Y, Li G, Zhang Y, Chen Z-Y. Experimental investigation into methane hydrate decomposition during three-dimensional thermal huff and puff. Energy Fuels 2011;25(4):1650–8.
[16] Myshakin EM, Anderson BJ, Rose K, Boswell R. Simulations of variable bottomhole pressure regimes to improve production from the double-unit mount elbert, milne point unit, north slope Alaska hydrate deposit. Energy Fuels 2011;25(3):1077–91.
[17] Huang L, Su Z, Wu N-Y. Evaluation on the gas production potential of different lithological hydrate accumulations in marine environment. Energy 2015;91:782–98.
[18] Li G, Li X-S, Wang Y, Zhang Y. Production behavior of methane hydrate in porous media using huff and puff method in a novel three-dimensional simulator. Energy 2011;36(5):3170–8.
[19] Li X-S, Li B, Li G, Yang B. Numerical simulation of gas production potential from permafrost hydrate deposits by huff and puff method in a single horizontal well in Qilian Mountain, Qinghai province. Energy 2012;40(1):59–75.
[20] Han D, Wang Z, Song Y, Zhao J, Wang D. Numerical analysis of depressurization production of natural gas hydrate from different lithology oceanic reservoirs with isotropic and anisotropic permeability. J Nat Gas Sci Eng 2017;46:575–91.
[21] Fujii T, Suzuki K, Takayama T, Tamaki M, Komatsu Y, Konno Y, et al. Geological setting and characterization of a methane hydrate reservoir distributed at the first offshore production test site on the Daini-Atsumi Knoll in the eastern Nankai Trough, Japan. Mar Petrol Geol 2015;66:310–22.
[22] Bhade P, Phirani J. Gas production from layered methane hydrate reservoirs. Energy 2015;82:686–96.
[23] Myshakin EM, Ajayi T, Anderson BJ, Seol Y, Boswell R. Numerical simulations of depressurization-induced gas production from gas hydrates using 3-D heterogeneous models of L-Pad, Prudhoe Bay Unit, North Slope Alaska. J Nat Gas Sci Eng 2016;35:1336–52.
[24] Lai K-H, Chen J-S, Liu C-W, Hsu S-Y, Steefel C. Effect of medium permeability anisotropy on the morphological evolution of two non-uniformities in a geochemical dissolution system. J Hydrol 2016;533:224–33.
[25] Su Z, He Y, Wu N, Zhang K, Moridis GJ. Evaluation on gas production potential from laminar hydrate deposits in Shenhu Area of South China Sea through depressurization using vertical wells. J Petrol Sci Eng 2012;86–87:87–98.
[26] Chen L, Feng Y, Kogawa T, Okajima J, Komiya A, Maruyama S. Construction and simulation of reservoir scale layered model for production and utilization of methane hydrate: the case of Nankai Trough Japan. Energy 2018;143:128–40.
[27] Yamamoto K, Dallimore S. Aurora-JOGMEC-NRCan Mallik 2006-2008 gas hydrate research project progress. Natural Gas & Oil. 2008;304:285–4541.
[28] Zhao J, Yu T, Song Y, Liu D, Liu W, Liu Y, et al. Numerical simulation of gas production from hydrate deposits using a single vertical well by depressurization in the Qilian Mountain permafrost, Qinghai-Tibet Plateau, China. Energy 2013;52:308–19.
[29] Yang S, Lang X, Wang Y, Wen Y, Fan S. Numerical simulation of Class 3 hydrate reservoirs exploiting using horizontal well by depressurization and thermal co-stimulation. Energy Convers Manag 2014;77:298–305.
[30] Saeki T, Fujii T, Inamori T, Kobayashi T, Hayashi M, Nagakubo S, et al. Extraction of methane hydrate concentrated zone for resource assessment in the eastern Nankai Trough, Japan. Offshore technology conference. Houston, Texas, USA: Offshore Technology Conference; 2008.
[31] Natural Gas Hydrates. Energy resource potential and associated geologic hazards. 2009.
[32] Kida M, Jin Y, Watanabe M, Konno Y, Yoneda J, Egawa K, et al. Chemical and crystallographic characterizations of natural gas hydrates recovered from a production test site in the eastern Nankai Trough. Mar Petrol Geol 2015;66:396–403.
[33] Fujii T, Nakamizu M, Tsuji Y, Namikawa T, Okui T, Kawasaki M, et al. Methane-hydrate occurrence and saturation confirmed from core samples. 2009. Eastern Nankai Trough, Japan.
[34] U.S. Geological Survey. USGS gas hydrates Project hosts Japanese colleagues to advance collaboration on Nankai Trough hydrate-bearing pressure cores. 2014. http://soundwaves.usgs.gov/2014/08/meetings.html/ [accessed August 2018].
[35] Sun J, Ning F, Zhang L, Liu T, Peng L, Liu Z, et al. Numerical simulation on gas production from hydrate reservoir at the 1st offshore test site in the eastern Nankai Trough. J Nat Gas Sci Eng 2016;30:64–76.
[36] Gupta A, Moridis GJ, Kneafsey TJ, Sloan ED. Modeling pure methane hydrate dissociation using a numerical simulator from a novel combination of X-ray computed tomography and macroscopic data. Energy Fuels 2009;23(12):5958–65.
[37] Moridis GJ, Collett TS, Dallimore SR, Satoh T, Hancock S, Weatherill B. Numerical studies of gas production from several CH4 hydrate zones at the Mallik site, Mackenzie Delta, Canada. J Petrol Sci Eng 2004;43(3):219–38.
[38] Li B, Liang Y-P, Li X-S, Wu H-J. Numerical analysis of methane hydrate decomposition experiments by depressurization around freezing point in porous media. Fuel 2015;159:925–34.

[39] Moridis GJ. TOUGH+ HYDRATE v1. 2 User's manual: a code for the simulation of system behavior in hydrate-bearing geologic media. 2012.
[40] Zhao J, Zhu Z, Song Y, Liu W, Zhang Y, Wang D. Analyzing the process of gas production for natural gas hydrate using depressurization. Appl Energy 2015;142:125–34.
[41] Moridis GJ, Reagan MT. Estimating the upper limit of gas production from Class 2 hydrate accumulations in the permafrost: 1. Concepts, system description, and the production base case. J Petrol Sci Eng 2011;76(3–4):194–204.